ELSEVIER

Chemical Geology 190 (2002) 69–89

CHEMICAL GEOLOGY
INCLUDING
ISOTOPE GEOSCIENCE

www.elsevier.com/locate/chemgeo

Determining mineral weathering rates based on solid and solute weathering gradients and velocities: application to biotite weathering in saprolites

Art F. White*

US Geological Survey, MS 420, 345 Middlefield Road, Menlo Park, CA 9402, USA

Abstract

Chemical weathering gradients are defined by the changes in the measured elemental concentrations in solids and pore waters with depth in soils and regoliths. An increase in the mineral weathering rate increases the change in these concentrations with depth while increases in the weathering velocity decrease the change. The solid-state weathering velocity is the rate at which the weathering front propagates through the regolith and the solute weathering velocity is equivalent to the rate of pore water infiltration. These relationships provide a unifying approach to calculating both solid and solute weathering rates from the respective ratios of the weathering velocities and gradients. Contemporary weathering rates based on solute residence times can be directly compared to long-term past weathering based on changes in regolith composition. Both rates incorporate identical parameters describing mineral abundance, stoichiometry, and surface area.

Weathering gradients were used to calculate biotite weathering rates in saprolitic regoliths in the Piedmont of Northern Georgia, USA and in Luquillo Mountains of Puerto Rico. Solid-state weathering gradients for Mg and K at Panola produced reaction rates of 3 to 6×10^{-17} mol m^{-2} s^{-1} for biotite. Faster weathering rates of 1.8 to 3.6×10^{-16} mol m^{-2} s^{-1} are calculated based on Mg and K pore water gradients in the Rio Icacos regolith. The relative rates are in agreement with a warmer and wetter tropical climate in Puerto Rico. Both natural rates are three to six orders of magnitude slower than reported experimental rates of biotite weathering.

Keywords: Mineral weathering rates; Biotite weathering; Saprolites

1. Introduction

The chemical weathering rates of silicate minerals are important in a number of geochemical processes, including soil nutrient cycling (Huntington et al., 2000), neutralization of acidic precipitation in watersheds (Drever and Hurcomb, 1986) and long-term draw-down of atmospheric CO_2 (Berner and Berner, 1997). Most natural silicate weathering rates are derived from relatively simple input–output calculations. Short-term weathering rates are calculated from changes in solute compositions in pore water, ground water or surface water over residence times of years to thousands of years (White and Claassen, 1978; Velbel, 1985; Paces, 1986; Kenoyer and Bowser, 1992; Swoboda-Colberg and Drever, 1993; Murphy et al., 1998). Long-term reaction rates are calculated from the differences between elemental or mineral compositions in the initial protolith and the weathered regolith

* Tel.: +1-650-329-4519; fax: +1-650-329-4538.
E-mail address: afwhite@usgs.gov (A.F. White).

0009-2541/02/$ - see front matter © 2002 Elsevier Science B.V. All rights reserved.
PII: S0009-2541(02)00111-0

(Sverdrup and Warfvinge, 1995; White et al., 1996). These rates are averages for the duration of regolith development, commonly thousands to millions of years.

No internally consistent approach presently exists to calculate and compare short- and long-term weathering rates using the above approaches. This paper addresses this deficiency by presenting a systematic methodology for calculating weathering rates based on solid and solute chemical distributions in soil/regolith profiles. The paper applies this synthesis to biotite weathering in saprolites and discusses the role of various geochemical and hydrologic parameters used in estimating chemical weathering rates.

2. Methodology

The chemical weathering rate R (mol m^{-2} s^{-1}) of a mineral can be expressed as

$$R = \frac{\Delta M}{St} \tag{1}$$

where ΔM is the mass of mineral reacted (mol m^{-3}), S is the volumetric surface (m^2 m^{-3}) and t is reaction time (s). In studies of soils and regoliths, the most direct evidence for chemical weathering is found in solid-state elemental and mineralogical changes with depth. In the simplest scenario for steady-state weathering, a mobile element, not incorporated into secondary precipitates, linearly decreases with decreasing depth from an initial concentration C_0 at depth z_1 to a concentration C_w at a shallower depth z_0 (Fig. 1). In weathering studies, solid concentrations are commonly reported as mol kg^{-1}. Mobilization from the solid also produces a corresponding linear increase in the same element in the pore water from c_0 at a depth of z_0 to c_w at depth z_1. Solute concentrations are most commonly expressed in terms of mol l^{-1}. A list of parameters used in the following derivations is presented in Table 1.

2.1. Calculation of solute concentrations

Changes in the solid and solute concentrations of an element due to weathering under completely closed system conditions can be expressed by the mass balance expression (after Velbel, 1986)

$$c_w - c_0 = \alpha\eta\rho_w\left[\sum_{j=1}^{m}\Delta C_j\beta_j - \sum_{k=1}^{n}\Delta C_k\beta_k\right] \tag{2}$$

The initial pore water concentration c_0 is commonly defined by recharge at the surface of the regolith as precipitation. The difference between the weathered solute concentration c_w and c_0 is the elemental weathering input from solid. ΔC_j (mol kg^{-1}) is the change in the solid element concentration due to weathering of primary mineral phase j and ΔC_k

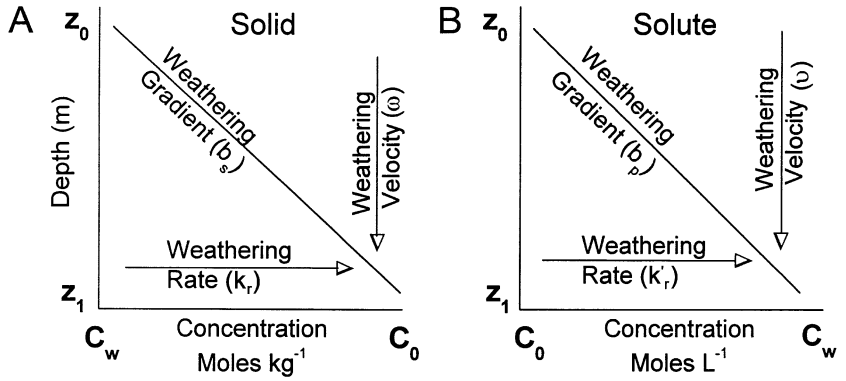

Fig. 1. Schematic showing the (A) solid and (B) solute distributions of a mobile element in a weathering regolith. C_w defines the solid weathered concentration at shallow depth z_0 and C_0 is the initial protolith concentration at depth z_1. c_w defines the corresponding solute weathered concentration and c_0 is the initial solute concentration. The weathering gradients b_s and b_p, which describe the solid and solute elemental distributions, are defined in terms of respective weathering rate (R_s and R_p) and velocity (ω and υ) vectors.

Table 1
List of parameters used in the paper

Symbol	Definition	Units
b_s	Slope of solid-state weathering gradient	m kg mol^{-1}
b_w	Slope of solute weathering gradient	m l mol^{-1}
C	Measured elemental concentration in solid	mol kg^{-1}
C_0	Elemental concentration in protolith	mol kg^{-1}
C_w	Elemental concentration in regolith	mol kg^{-1}
c_0	Initial elemental concentration in solute	mol l^{-1}
c_w	Final elemental concentration in solute	mol l^{-1}
I_0	Conservative elemental concentration in protolith	mol kg^{-1}
I_w	Conservative element concentration in regolith	mol kg^{-1}
ΔM_s	Mass of mineral reacted in regolith based on solid-state composition	mol m^{-3}
ΔM_p	Mass of mineral reacted in regolith based on solute composition	mol m^{-3}
Δm_s	Solid-state element change	m s^{-1}
Δm_p	Solute element change	mol m^{-3}
q_h	Fluid flux density	mol m^{-3}
R_s	Surface-normalized weathering rate based on solid-state gradient	mol $m^{-2}s^{-1}$
R_p	Surface-normalized weathering rate based on solute gradient	mol $m^{-2}s^{-1}$
r_s	Volume-normalized weathering rate based on solid-state gradient	mol m^{-3} s^{-1}
r_p	Volume-normalized weathering rate based on solute gradient	mol m^{-3} s^{-1}
S	Volumetric mineral surface area	m^2 m^{-3}
s	Specific mineral surface area	m^2 g^{-1}
t_s	Duration of regolith weathering	s
t'	Solute residence time	s
V_0	Protolith volume	m^3
V_w	Regolith volume	m^3
z	Regolith depth	m
α	Regolith porosity	m^3 m^{-3}
β	Stoichiometric coefficient for elemental distribution in mineral	mol mol^{-1}
η	Fluid saturation	m^3 m^{-3}
ρ_0	Protolith specific density	g cm^{-3}
ρ_w	Regolith specific density	g cm^{-3}
υ	Solute weathering velocity	m s^{-1}
ω	Solid state weathering velocity	m s^{-1}

(mol kg^{-1}) is the elemental change due to uptake in the secondary mineral phase k. β_j and β_k are the stoichiometric coefficients that define the number of moles of the element present in a mole of the respective mineral phase. The number of primary mineral phases contributing the change in element concentration in the pore water is m and the number of secondary minerals depleting the element is n. The parameters outside the brackets on the right side of Eq. (2) are the conversion factors that relate molar element concentrations in the solid to the solute where ρ_w (kg m^{-3}) is the regolith density, α is the regolith porosity (m^3 m^{-3}) and η (m^3 m^{-3}) is the fluid saturation factor ($\eta = 1$ for saturated conditions). These parameters define the physical state of the regolith.

The sequence of linear simultaneous equations generated by Eq. (2) can be solved sequentially for a number of elements and minerals using a spread sheet (Garrels and Mackenzie, 1967; Velbel, 1985) or a computer program such as NETPATH (Plummer et al., 1991). In either case, the calculations are constrained by the number of elements considered and the number and changes in the elemental concentrations in the primary and secondary minerals. The extent to which the change in measured pore water elemental concentrations in Eq. (2) actually reflects that chemical weathering is also dependent by the magnitude of other geochemical processes occurring in the regolith. These include evapotranspiration, elemental cycling by vegetation and ion exchange.

2.2. Calculation of solid-state concentrations

During in situ weathering, the initial solid elemental concentration C_0 shown in Fig. 1 is assumed to be that of the bedrock or protolith. For regoliths formed in deposits such as alluvium, the determination of C_0 becomes more difficult and is generally assumed to be the least weathered sample taken at the greatest depth. C_w is the elemental concentration at a shallower depth in the regolith, which reflects chemical weathering. Under closed system conditions, the total mass change in solid-state regolith reflected in the difference in concentrations C_0-C_w is balanced directly by mass changes in solute concentrations reflected by c_w-c_0 (Eq. (2)). However, for most natural weathering, open system conditions apply and the total concentration change in the regolith over long weathering times is expected to be many orders of magnitude greater than the changes in the solute during relatively short pore water residence times.

In most studies, the solid-state element concentration C_w, reflecting weathering, cannot be determined directly from the measured elemental concentration C, i.e. $C_w \neq C$. This is because the measured concentration C is dependent on mass and density changes produced from loses or gains of other elements during weathering and volume changes caused physical collapse or dilation of the regolith. The most common method for correcting for such physical changes in the regolith is to consider an additional element that is inert to chemical weathering such as Ti, Zr and Nb (White, 1995). The normalized weathering concentration C_w, defining the weathering profile in Fig. 1, is obtained from the measured concentration C by the relationship

$$C_w = C\left(\frac{I_0}{I_w}\right) \tag{3}$$

where I_0 (mol kg^{-1}) is the concentration of the inert element in the protolith and I_w is the concentration in the weathered regolith. If the inert concentrations are the same, i.e. $I_0/I_w = 1$, the measured and normalized concentrations of the weatherable element are also the same and $C_w = C$. If $I_0/I_w < 0$, the measured concentration of the mobile element will be greater than the normalized weathered concentration, i.e. $C > C_w$. If $I_0/I_w > 1$, then the normalized concentration will be less, i.e. $C < C_w$.

2.3. Mass changes due to weathering

In order to make direct comparisons of element mobility due to weathering, changes in molar densities in the solid Δm_s (mol m^{-3}) and pore water Δm_p (mol m^{-3}) are defined in terms of a unit regolith volume such that

$$\Delta m_s = 1000\rho_w(C_w - C_0) \tag{4}$$

and

$$\Delta m_p = 1000\alpha\eta(c_w - c_0) \tag{5}$$

The value of 1000 in Eq. (4) is the conversion factor between bulk density (g cm^{-3}) and the SI density unit (kg m^{-3}). The value of 1000 in Eq. (5) is the conversion factor between 1 and the SI unit for fluid volume (m^3). Note that the elemental change in the solid (Eq. (4)) is negative because the weathered concentration C_w is less than the initial protolith concentration C_0 (Fig. 1). In contrast, the change in chemical concentration in the pore water is positive because the initial solute concentration c_0, is less than the final concentration c_w.

Changes in solid and solute elemental concentrations (Eqs. (4) and (5)) can be converted to changes in mineral molar densities ΔM_s and ΔM_p (mol m^{-3}) by dividing by the stoichiometric coefficient for the mineral β (Eq. (2)) such that

$$\Delta M_s = 1000\frac{\rho_w}{\beta}(C_w - C_0) \tag{6}$$

and

$$\Delta M_p = 1000\frac{\alpha\eta}{\beta}(c_w - c_0) \tag{7}$$

ΔM_s and ΔM_p define the mass of mineral reacted in the initial kinetic rate expression (Eq. (1)). Under completely closed system conditions, the changes in elemental and mineral concentrations are conservative and losses in the solid are equal to gains in the solute, i.e. $\Delta m_s + \Delta m_p = 0$ (Eqs. (4) and (5)) and $\Delta M_s + \Delta M_p = 0$ (Eqs. (6) and (7)). This is identical to the

mass balance relationship expressed in Eq. (2). However, in most natural open system weathering situations, the mass loss in the solid is much greater than the mass gain in the solute, i.e. $|\Delta m_s| \gg |\Delta m_p|$ and $|\Delta M_s| \gg |\Delta M_p|$.

2.4. Weathering gradients

The respective changes in chemical concentrations in the solid and the solute are defined spatially with depth in the regolith by the weathering gradients (Fig. 1). The slope of the solid-state weathering gradient is defined as b_s (m kg mol^{-1}) and the solute gradient as b_p (m l mol^{-1}). Therefore, $C_w - C_0 = \Delta z/b_s$ and $c_w - c_0 = \Delta z/b_p$. Substituting these relationships into Eqs. (6) and (7) results in the expressions

$$\Delta M_s = 1000\frac{\rho_w}{\beta}\left(\frac{\Delta z}{b_s}\right) \quad (8)$$

and

$$\Delta M_p = 1000\frac{\alpha\eta}{\beta}\left(\frac{\Delta z}{b_p}\right) \quad (9)$$

As defined in Eqs. (8) and (9), the extent of mass loss is inversely proportional to weathering gradient b, the shallower the weathering gradient; the greater will be the elemental loss. This inverse relationship is a result of the common convention in which depth is plotted on the vertical scale and the dependent concentration variable is plotted on the horizontal axis (Fig. 1).

2.5. Weathering velocities

The masses of reacted mineral, based on solid-state and solute weathering, are define in Eqs. (8) and (9) in terms of the spatial dimension, z, which is the regolith depth. However, such masses can also be defined in terms of the temporal dimension t (s) as is required for the initial weathering rate expression (Eq. (1)). This is done by defining a weathering velocity, which for the solid state is ω (m s^{-1}) $= \Delta z/t_s$ and for the solute is v (m s^{-1}) $= \Delta z/t_p$. Over relatively short pore water residence times t_p, the weathering velocity v is rapid and there is no significant change in mineral content. Therefore, the vertical position of the solute weathering gradient will be fixed with respect to z over time (Fig. 1). The weathering velocity ω, associated with solid-state changes in the regolith, commonly involves much longer times t_s over which significant changes in mass occurs. The position of the solid-state weathering gradient will move progressively downward through the regolith with increasing times. However, as long as steady-state weathering conditions persist, the slope of the concentration/depth relationship which defines the weathering gradients b_s and b_p will remain constant with time (Fig. 1).

Substituting the weathering velocities ω and v for Δz in Eqs. (8) and (9) and dividing both sides of the respective expressions by t_s and t_p produce expressions describing the mineral weathering rate per unit volume of regolith r_s and r_p (mol m^{-3} s^{-1}) such that

$$r_s = 1000\frac{\rho_w}{\beta}\left(\frac{\omega}{b_s}\right) \quad (10)$$

and

$$r_p = 1000\frac{\alpha\eta}{\beta}\left(\frac{\upsilon}{b_p}\right) \quad (11)$$

Note that the slopes of the weathering gradients b_s and b_p are inversely proportional to the weathering rates (Fig. 1). Thus, faster weathering rates will diminish the weathering gradients, i.e. the slopes of the diagonal lines in Fig. 1 will decrease. Consequently, observed changes in solid-state or pore water concentrations in the field will be large over a given depth interval. Conversely, a decrease in the weathering rate will increase the weathering gradients so that the observed changes in concentration will be less pronounced with depth.

The solute weathering velocity v is expressed as the rate of water movement through the pore spaces in the regolith, i.e. v (m s^{-1}) $= \Delta z/t_p$. In order to calculate the mass of water and, therefore, solute transported through a given volume of regolith (m^3), this velocity must be adjusted for the porosity ρ and fluid saturation η of the regolith (Eq. (11)). Fluid transport is more commonly measured as flux density q_h (m s^{-1}), which is the volume of water (m^3) moving across a given cross-section of regolith (m^2) (Hillel, 1982). While q_h is expressed in the same units as υ (m s^{-1}), the flux density is intrinsic to the medium through which the fluid is transported. Under such conditions, and assuming no hydrologic dispersion,

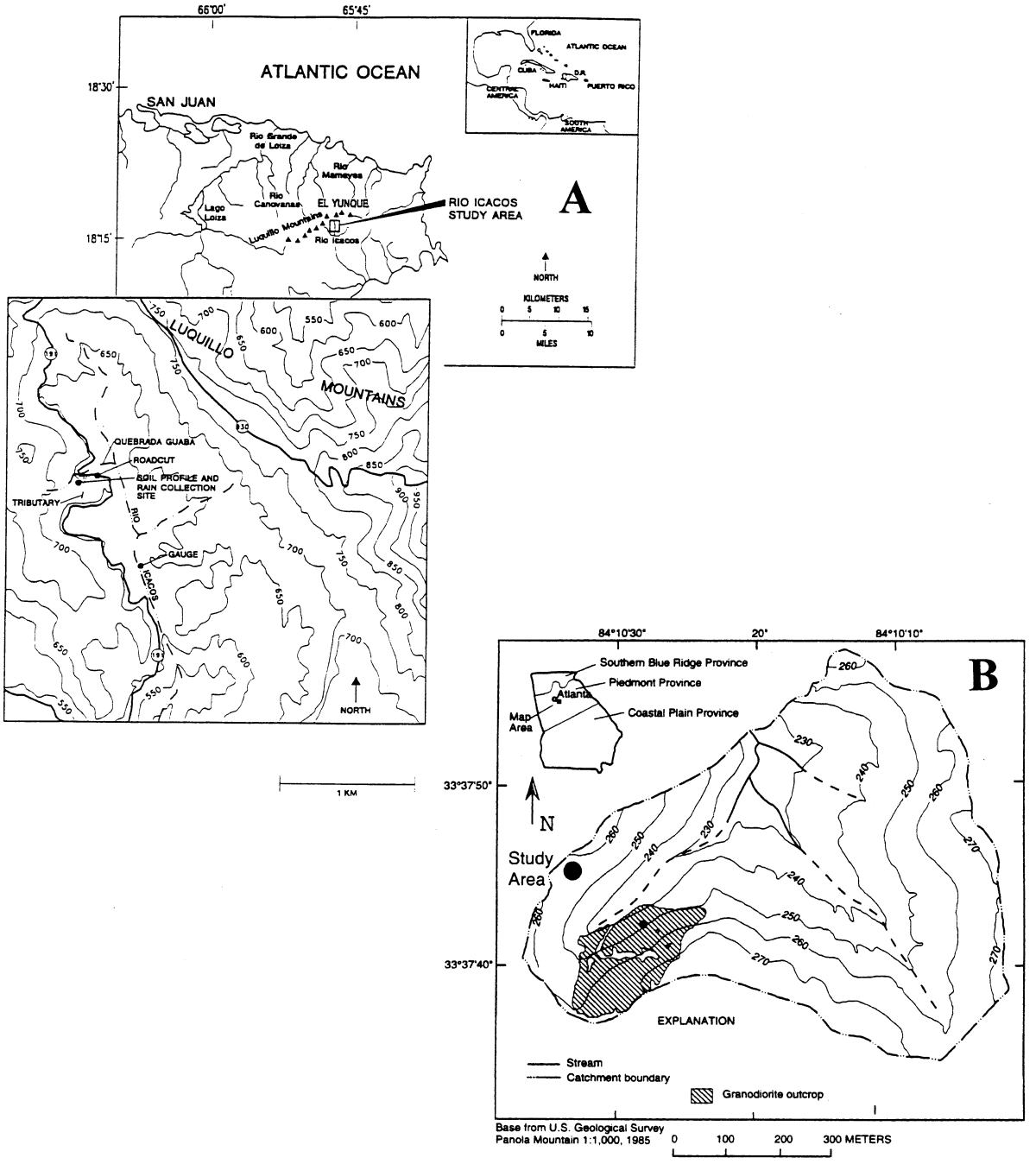

Fig. 2. Maps showing the locations and topographic features of the (A) Rio Icacos and (B) Panola watersheds.

$q_h = \alpha\eta v$, the porosity and fluid saturation terms are eliminated from Eq. (11) such that

$$r_p = 1000\frac{1}{\beta}\left(\frac{q_h}{b_p}\right) \quad (12)$$

2.6. Surface areas

The above mineral weathering rates r_s and r_p are defined in terms of a unit volume of regolith and are not normalized to the mass of a mineral phase present. More useful weathering rates, which can be directly compared to weathering in other environments, are produced by dividing Eqs. (10) and (12) by the total surface area of a mineral contained in a unit volume of regolith S ($m^2\ m^{-3}$)

$$R_s = 1000\frac{\rho_w}{S\beta}\left(\frac{\omega}{b_s}\right) \quad (13)$$

and

$$R_p = 1000\frac{1}{S\beta}\left(\frac{q_h}{b_p}\right) \quad (14)$$

R_s and R_p (mol $m^{-2}\ s^{-1}$) are equivalent to the original rate equation describing mineral weathering (Eq. (1))

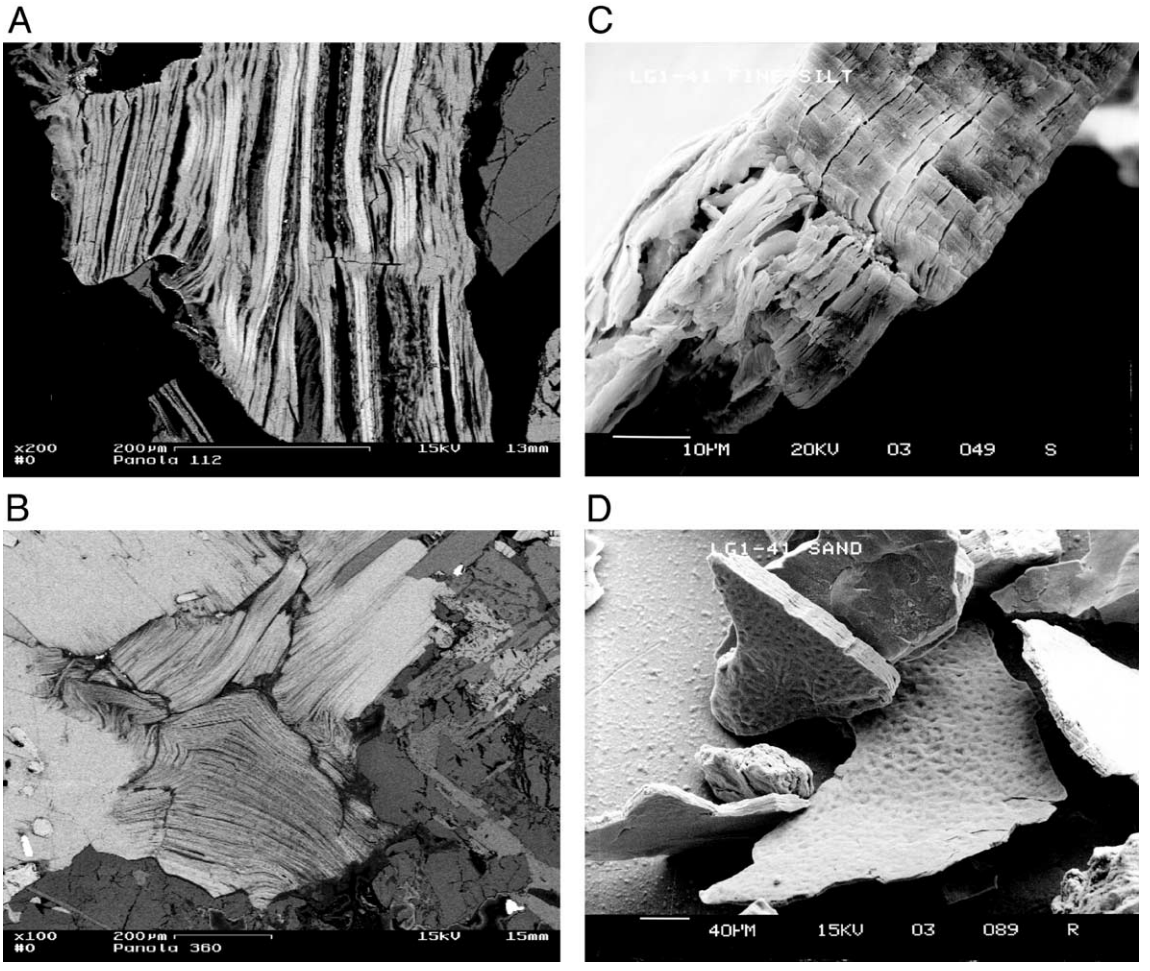

Fig. 3. Back-scattered electron images of biotite weathering. (A) Altered biotite from a depth of 3 m in the Panola saprolite. In this thin section, biotite shows up as bright areas corresponding to higher mean atomic numbers and interlayer kaolinite as the gray areas. (B) Altered biotite from a depth of 9 m in weathered Panola granodiorite. Note the separation and fanning of kaolinized layers. (C) Pseudomorphic replacement of a biotite grain by kaolinite at a depth of 1 m in the Rio Icacos saprolite. (D) Altered biotite grains from a depth of 0.5 m in the Rio Icacos saprolite. The bumpy texture is indicative of near-complete epitaxial replacement by kaolinite.

Table 2
Mineralogy and compositions of Panola and Rio Icacos weathering profiles (wt.%).

Mineral	Formula	Bed-rock	Saprolite	Saprolite	Soil B Horz.
Panola		11.5 m	4.8 m	2.5 m	1.0 m
Biotite (rock)	$K_{0.98}(Mg_{0.89}Fe(II)_{1.53}Al_{0.26}Ti_{0.15})(Al_{1.20}Si_{2.80})O_{10}(OH)_2$	13.2	9.9	6.2	3.1
Muscovite	$K_{1.62}(Mg_{0.28}Fe(II)_{0.44}Al_{1.04}Ti_{0.10})(Al_{2.94}Si_{2.8})O_{10}(OH)_2$	6.7	6.7	6.7	6.7
Quartz	SiO_2[a]	28.7	38.4	38.9	35.8
Plagioclase	$Na_{0.77}Ca_{0.23}Al_{1.23}Si_{2.77}O_8$	31.4	5.5	1.1	2.3
K-feldspar	$Na_{0.03}K_{0.97}Al_{1.02}Si_{2.99}O_8$	20.0	16.2	16.8	11.6
Kaolinite	$Al_2Si_2O^{10}(OH)_4^a$	0.0	21.4	27.1	34.2
Fe oxides	FeO(OH)[a]	0.0	1.9	3.2	6.3
Rio Icacos		8.12 m	7.13 m	2.87 m	0.76 m
Biotite (rock)	$K_{0.85}(Al_{0.10}Ti_{0.20}Fe^{2+}_{1.30}Fe^{3+}_{0.05}Mg_{1.25})(Si_{2.8}Al_{1.2})O_{10}(OH)_2$	9.5	na	na	na
Biotite (regolith)	$K_{0.65}(Al_{1.10}Ti_{0.15}Fe^{2+}_{0.35}Fe^{3+}_{0.15}Mg_{0.55})(Si_{3.2}Al_{0.8})O_{10}(OH)_2$	na	16.2	18.6	21.1
Quartz	SiO_2^a	24.9	20.6	23.5	21.9
Plagioclase	$Na_{0.60}Ca_{0.40}Al_{1.36}Si_{2.63}O_8$	56.4	0.0	0.0	0.0
K-feldspar	$Na_{0.09}K_{0.91}AlSi_3O_8$	1.8	0.0	0.0	0.0
Hornblende	$(Na_{0.34},K_{0.05})(Ca_{1.71}Mg_{2.84}Fe_{2.06}Al_{0.89}[Al_{1.00}Si_{6.68}]O_{22}(OH)_2$	6.3	0.0	0.0	0.0
Kaolinite	$(K_{0.01}Fe_{0.07}Mg_{0.04})(Si_{2.21}Al_{1.69})O_5(OH)_4$	0.0	63.2	57.9	57.0
Goethite	FeO(OH)[a]	1.9	3.9	2.5	2.4

After Murphy et al. (1998), White et al. (1998), White et al. (2001); na = not applicable.
[a] Asummed compositions.

but are now expressed in terms of parameters directly measurable in weathered regoliths.

Surface areas are most commonly reported, such as in BET analyses, in terms of the mass of a specific mineral phase s ($m^2\ g^{-1}$) which is related to the volumetric surface area S by the relationship

$$s = \frac{S}{10^6 \phi \rho_w} \tag{15}$$

where ϕ is the mass fraction of the specific mineral in the regolith (kg kg^{-1}).

2.7. Parallel weathering rate equations

Substituting Eq. (15) into Eqs. (13) and (14) produces the final forms of the solid-state and solute reaction rates expressions

$$R_s = \frac{1}{1000}\left(\frac{1}{\phi\beta S}\right)\left(\frac{\omega}{b_s}\right) \tag{16}$$

and

$$R_p = \frac{1}{1000}\left(\frac{1}{\rho_w}\right)\left(\frac{1}{\phi\beta S}\right)\left(\frac{q_h}{b_p}\right) \tag{17}$$

The solid-state and solute weathering rate expressions (Eqs. (16) and (17)) exhibit very similar forms. Both rates are inversely proportional to the set of terms defining mineralogical properties, i.e. the mineral fraction ϕ, the mineral stoichiometry β and the specific mineral surface area s. These terms convert regolith elemental masses to mineral abundance expressed in terms of specific surface areas.

Both rate equations are proportional to the ratios of the weathering velocities to the weathering gradients. In Eq. (16), this ratio is the rate of regolith propagation ω divided by the rate at which the solid elemental concentration increases with depth (b_s) (Eq. (15)). For Eq. (17), the ratio is the hydraulic flux density q_h divided by the increase in solute concentration with depth (b_p). During steady-state weathering under open conditions, the magnitude of the elemental and mineral changes in the solid are orders of magnitude greater than for the solute $|\Delta m_s| \gg |\Delta m_p|$ and $|\Delta M_s| \gg |\Delta M_p|$ (Eqs. (4)–(9)). However, the reaction rates are equal, $R_s = R_p$ (Eqs. (16) and (17)). This equality forms the basis for comparing contemporary short-term weathering rates with past long-term rates.

2.8. Application to biotite weathering in saprolites

The preceding rate calculations based on solid and solid elemental gradients (Eqs. (16) and (17)) are applied to biotite weathering in two saprolitic regoliths located in the semitropical Panola watershed in Piedmont Province of Northern Georgia, USA (White et al., 2002) and in the tropical Rio Icacos watershed in the Luquillo Mountains of eastern Puerto Rico (Murphy et al., 1998; White et al., 1998) (Fig. 2). Saprolite is defined as a clay-rich, decomposed crystalline rock that retains evidence of parent bedrock textures. Saprolites are developed in situ from crystalline bedrock and have been subjected to isovolumetric weathering involving significant mass losses. These features make for long-term steady-state conditions optimal for characterizing chemical weathering based on solid and solute elemental gradients (Eqs. (16) and (17)).

Both the Panola and Rio Icacos regoliths are situated on stable ridge tops comprising old geomorphic surfaces (2 to 5×10^5 years; Brown et al., 1995; Bierman et al., 1995). The Panola regolith consists of an unstructured ultisol (1.5 m thick) underlain by a porous saprolite ($\sim 2-3$ m thick), which retains the original bedrock texture. This saprolite grades to competent but weathered Panola Granite (granodiorite) at a depth of 4.7 m. Unweathered granite is present at a depth of 8 m. The Rio Icacos regolith consists of a highly weathered ultisol up to 1.5 m thick underlain by 6- to 8-m thick saprolite formed from the Rio Blanco quartz diorite.

3. Results

Much of the chemical and hydrologic data for Panola and Rio Icacos regoliths are based on previous work cited above but are recast and reinterpreted in terms of the rate expressions derived in the present study (Eqs. (15) and (16)).

3.1. Stoichiometry of biotite weathering

The determinations of mineral weathering rates from solid and solute elemental weathering gradients require defining reactions in terms of the stoichiometric coefficient β which partitions elemental molar

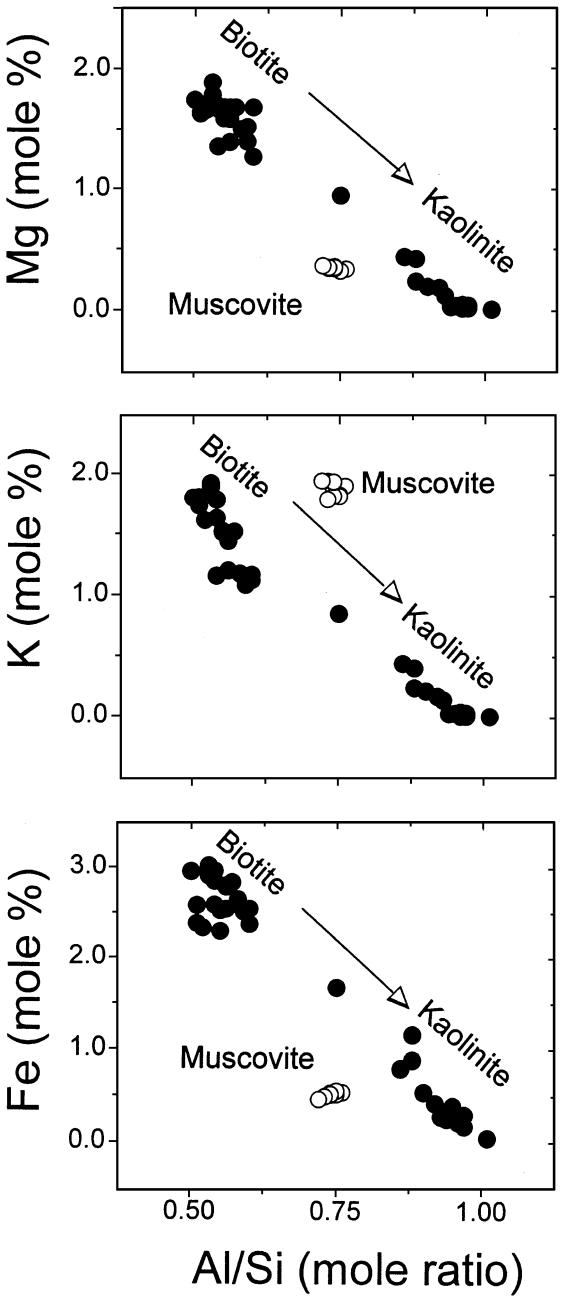

Fig. 4. Changes in Mg, K and Fe mol% with Al/Si molar ratios in biotite and muscovite grains as functions of weathering in the Panola regolith. Arrows denote composition trends resulting from the progressive pseudomorphic replacement of biotite by kaolinite.

concentrations between the solid and solute phases (Eq. (2)). While a vermiculite intermediary sometimes occurs (Banfield and Eggleton, 1988), kaolinite is the most common alteration product of biotite formed during intense weathering in semitropical and tropical climates such as in the Panola and Rio Icacos watersheds (Dong et al., 1998; Murphy et al., 1998; White et al., 2002).

Such replacement is shown in Fig. 3, in which relatively large biotite books are partially to completely altered by pseudomorphic replacement with kaolinite. TEM observations for the Rio Icacos phllyosilicate books indicate direct epitaxial replacement with one biotite layer terminating against two layers of kaolinite (Murphy et al., 1998). The dark and light interlayers in weathered Panola biotite (Fig. 3A and B) are also distinct compositionally with Al/Si ratios approaching 0.5 for fresh biotite and ratios approaching 1.0, which is representative of kaolinite (Table 2). The increase in Al/Si ratios correlates with loss of K from interlayer sites and Mg from octahedral sites. Fe is also oxidized and lost from the biotite structure (Fig. 4).

The epitaxial weathering of biotite to kaolinite, assuming Al conservation, is written for the Panola regolith as (White et al., 2002)

$$\begin{aligned} &K_{0.98}(Mg_{0.89}Fe(II)_{1.53}Al_{0.26}Ti_{0.15}) \\ &\quad\times(Al_{1.20}Si_{2.80})O_{10}(OH)_2 + 2.78H^+ \\ &\quad + 0.38O_2 + 2.99H_2O \\ &\quad\rightarrow 0.73Al_2Si_2O_5(OH)_4 + 1.53FeOOH \\ &\qquad + 0.98K^+ + 0.89Mg^{2+} + 1.34H_4SiO_4 \\ &\qquad + 0.15TiO_2 \end{aligned} \tag{18}$$

This reaction is based on the biotite composition in the unweathered Panola Granite (Table 2). The resolution of the microprobe analyses was insufficient to completely separate compositions of individual biotite layers from adjacent kaolinized layers in the weathered phyllosilicate books. Although the composition of the biotite weathering in the regolith is not known, the elemental trends in Fig. 4 indicate that this biotite

Table 3
Measured (C) and normalized (C_w) elemental concentrations (mol kg^{-1}), bulk densities (ρ, g cm^{-3}), and biotite contents of the Panola and Rio Icacos protolith and regoliths (data from White et al., 1998, 2002)

Depth (m)	ρ	Mg, C	K, C	Ti, C	Mg, C_w	K, C_w	Biotite, weight fraction	Depth (m)	ρ	Mg, C	K, C	Ti, C	Mg, C_w	K, C_w	Biotite, weight fraction
Panola Granodiorite								*Rio Icacos Quartz Diorite*							
na	2.50	0.251	1.008	0.152	0.251	1.008	0.130	na	2.70	0.422	0.197	0.039	0.422	0.197	0.10
Panola Regolith								*Rio Icacos Regolith*							
0.10	1.95	0.051	0.648	0.299	0.026	0.329	0.010	0.25	0.84	0.037	0.161	0.068	0.022	0.093	0.030
0.30	1.86	0.077	0.723	0.235	0.050	0.467	0.040	0.48	1.09	0.020	0.159	0.061	0.024	0.102	0.030
0.48	1.86	0.124	0.596	0.217	0.087	0.418	0.070	0.56	1.15	0.182	0.415	0.075	0.095	0.216	0.140
0.74	1.83	0.096	0.648	0.168	0.087	0.585	0.050	0.76	1.29	0.372	0.188	0.061	0.024	0.121	0.150
0.84	1.73	0.109	0.559	0.189	0.088	0.449	0.060	1.04	1.39	0.140	0.278	0.062	0.088	0.175	0.100
1.07	1.81	0.121	0.535	0.198	0.093	0.411	0.060	1.35	1.43	0.146	0.267	0.078	0.073	0.135	0.110
1.27	1.83	0.119	0.554	0.182	0.099	0.461	0.060	2.03	1.38	0.110	0.271	0.061	0.070	0.172	0.080
1.52	1.78	0.111	0.455	0.169	0.099	0.408	0.060	2.31	1.33	0.179	0.417	0.082	0.085	0.199	0.130
1.83	1.80	0.096	0.563	0.188	0.077	0.454	0.050	2.54	1.30	0.151	0.294	0.085	0.069	0.134	0.110
2.16	1.72	0.132	0.668	0.189	0.106	0.537	0.070	2.59	1.29	0.166	0.367	0.105	0.062	0.137	0.120
2.51	1.99	0.185	0.679	0.204	0.137	0.504	0.100	2.87	1.27	0.161	0.392	0.073	0.086	0.210	0.120
2.84	2.25	0.202	0.937	0.208	0.147	0.683	0.110	3.23	1.25	0.167	0.388	0.074	0.088	0.204	0.120
3.23	1.97	0.292	1.048	0.233	0.190	0.682	0.160	3.63	1.26	0.176	0.400	0.074	0.092	0.210	0.130
3.73	2.06	0.264	0.852	0.191	0.209	0.676	0.140	4.52	1.35	0.159	0.470	0.079	0.079	0.233	0.120
3.99	2.00	0.243	0.888	0.199	0.185	0.675	0.130	5.05	1.41	0.183	0.443	0.079	0.090	0.219	0.140
4.29	2.00	0.224	0.649	0.157	0.216	0.627	0.120	6.12	1.42	0.176	0.417	0.079	0.087	0.207	0.130
4.52	2.00	0.229	0.840	0.199	0.175	0.642	0.120	7.14	1.22	0.188	0.470	0.088	0.083	0.208	0.140
4.65	2.00	0.270	0.878	0.197	0.209	0.677	0.140								

composition must be similar to the fresh bedrock biotite.

Based on microprobe and wet chemical analyses (Murphy et al., 1998), the composition of the fresh biotite in the parent Rio Blanco quartz diorite was determined to be $K_{0.85}(Mg_{1.25}Fe(II)_{1.30}Fe(III)_{0.05}Al_{0.10}Ti_{0.20})(Al_{1.20}Si_{2.80})O_{10}(OH)_2$ (Table 2). The application of scanning-transmission electron microscopy (STEM) increased the spatial resolution of the chemical analyses of the biotite/kaolinite intergrowths from the overlying regolith. These results indicated significantly lower K, Mg and Fe contents for weathered biotite component. This indicates that biotite preserved in the regolith had undergone prior partial weathering and oxidation in the bedrock or at the saprolite bedrock interface. The proposed biotite weathering reaction in the Rio Icacos saprolite is (Murphy et al., 1998)

$$\begin{aligned} &K_{0.65}(Mg_{0.55}Fe(II)_{0.35}Fe(III)_{0.15}Al_{1.10}Ti_{0.15}) \\ &\quad\times(Al_{0.80}Si_{3.20})O_{10}(OH)_2 + 1.62H^+ \\ &\quad + 0.08O_2 + 2.89H_2O \\ &\quad\rightarrow 0.95Al_2Si_2O_5(OH)_4 + 0.50FeOOH \\ &\qquad + 0.65K^+ + 0.55Mg^{2+} + 1.30H_4SiO_4 \\ &\qquad + 0.15TiO_2 \end{aligned} \quad (19)$$

During biotite weathering, Mg and K are the only elements completely mobilized from the solid to the solute phases (Eqs. (18) and (19)), thus serving as the basis on which biotite weathering rates are calculated (Eqs. (16) and (17)). The stoichiometric coefficients for Panola biotite weathering are $\beta_{Mg}=0.89$ and $\beta_K=0.98$ and for the Rio Icacos weathering $\beta_{Mg}=0.55$ and $\beta_K=0.65$ (Eq. (18)).

3.2. Solid-state weathering gradients

Complete solid-state analyses of the Rio Icacos and Panola and regoliths are presented by White et al. (1998, 2002). Measured Mg and K concentrations in the Panola and Rio Icacos regoliths are tabulated in Table 3 and plotted as functions of depth in Fig. 5. Concentrations in the basal Panola saprolite (4.8 m) are similar to the underlying fresh bedrock at a depth of 11.5 m. Mg is contained in biotite and to a lesser extent in muscovite (Table 3). As shown in Fig. 4 and discussed by White et al., 2002, muscovite is essentially unreactive in the Panola regolith, thus making changes in solid-state Mg concentrations dependent solely on biotite weathering. K is contained in biotite, muscovite and K-feldspar. As shown in Table 2, approximately 50% of the K-feldspar is lost compared to more than 75% of the biotite during regolith weathering. Most of K-feldspar weathering occurs near the bedrock/saprolite interface (White et al., 2002).

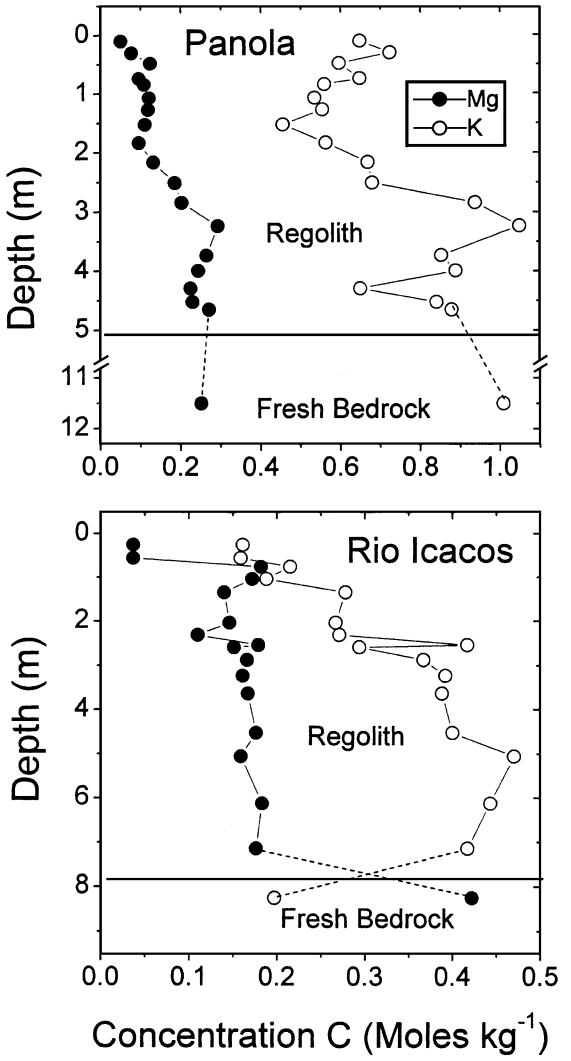

Fig. 5. Measured solid-state Mg and K concentrations in the Panola and Rio Icacos regoliths and protoliths. The weathered bedrock section in the Panola profile (5–11 m) is not shown.

Mg in Rio Icacos protolith is contained in biotite and hornblende (Table 2). Hornblende is completely weathered at the saprolite/bedrock interface (White et al., 1998). A comparison of biotite compositions indicates that more than 50% of the Mg is also lost from the biotite at the bedrock/saprolite interface (Table 2). Both of these processes account for much lower Mg concentrations in the saprolite compared to the underlying fresh bedrock (Fig. 5). K is contained in biotite and relatively small amounts of K-feldspar. The apparent increase in K in the saprolite relative to the bedrock reflects the condition that biotite and K-feldspar weather less rapidly than other minerals in the profile, particularly plagioclase (Table 2).

The normalized solid-state Mg and K concentrations in the Panola and Rio Icacos regoliths (C_w) are calculated from Eq. (3) using measured concentrations of Ti in the bedrocks and regoliths (Table 3). Ti is one of the several refractory elements shown to be inert to weathering in the Panola and Rio Icacos regoliths (White et al., 1998, 2002). The ratios I_0/I_w, plotted in Fig. 6A are significantly less than unity for the Panola (average $I_0/I_w = 0.77$) and Rio Icacos regoliths (average $I_0/I_w = 0.53$). Since Ti does not weather, the increases in Ti relative to the bedrock must reflect decreases in regolith density and/or volume. The density ratios ρ_0/ρ_w plotted in Fig. 6B are higher than unity indicating that the regolith densities are lower than the bedrock densities. The highest density ratios occur in the shallow Rio Icacos soil where the density approaches one third of that of bedrock (Table 3).

The volume changes in the regolith can be calculated from the ratios of the regolith to protolith densities and measured Ti concentrations (White et al., 1996)

$$\frac{V_0}{V_w} = \frac{\rho_0}{\rho_w}\frac{I_0}{I_w} \tag{20}$$

Changes in the volume ratios V_0/V_w in the Panola and Rio Icacos regoliths are negligible, except in the shallow soils (Fig. 6C). The lack of volume changes is characteristic of saprolitic regoliths, a feature that preserves the original bedrock texture (Velbel, 1990). Density changes without corresponding volume changes require significant mass losses due to chemical weathering. Higher I_0/I_w and ρ_0/ρ_w ratios indicate that the intensity of chemical weathering in the Rio Icacos regolith is significantly greater than in the Panola regolith, as expected for a warmer and wetter climate.

The normalized weathering concentrations of Mg and K in the Panola and Rio Icacos regoliths (C_w) are lower than the measured concentrations (C) (Table 3), indicating that Mg and K are concentrated in the regolith relative to other components. Solid Mg and K concentrations (C_w) exhibit strong linear correlations with depth in the Panola regolith (Fig. 7). These

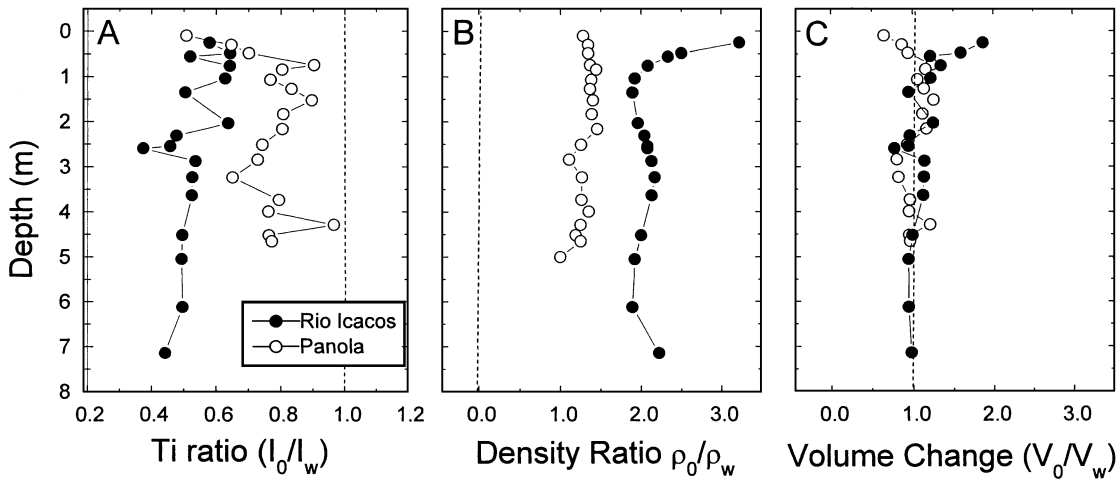

Fig. 6. Parameters used to characterize the extent of weathering in the Panola and Rio Icacos regoliths. (A) Concentration ratios of inert Ti in protolith I_0 and regolith I_w. (B) Density ratios of the protolith ρ_0 and regolith ρ_w. (C) Volume ratios of the protolith V_0 and regolith V_W. In each case, the vertical dashed line refers to the initial protolith condition.

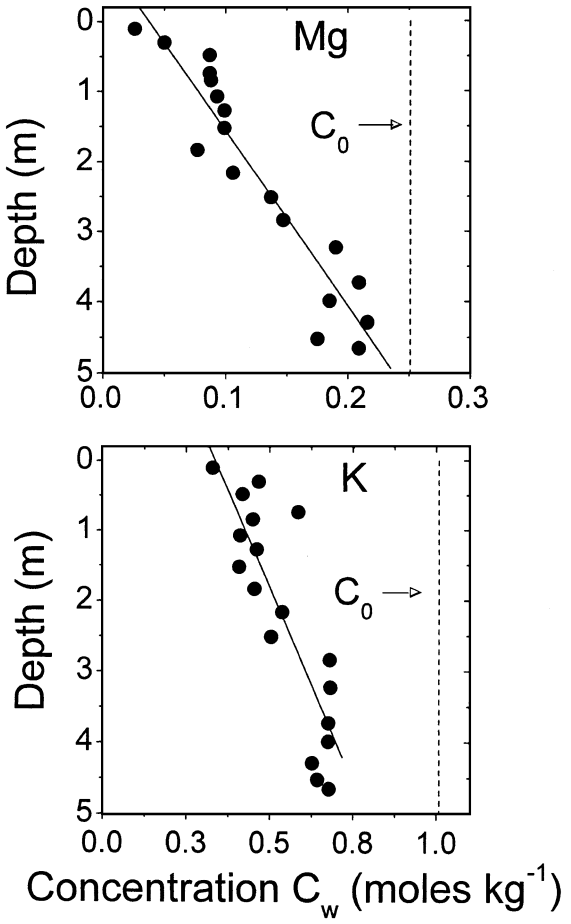

Fig. 7. Normalized solid concentrations of Mg and K (C_w) plotted as a function of depth in the Panola regolith. C_0 is the measured protolith concentrations (vertical dashed lines). The diagonal lines are the linear regression fits describing the solid-state weathering gradients b_s (Eq. (16)).

correlations are equivalent to solid-state weathering gradients defined in Fig. 1 and, based on the linear regression fits (diagonal lines), are determined to be $b_s = 25.0$ and 11.1 m $mol^{-1} kg^{-1}$ for Mg and K, respectively. The weathering rate, normalized to unit volume of saprolite, is inversely proportional to b_s. Therefore, K is released at a rate approximately twice as fast as Mg. This difference occurs because K is contained in the regolith in significantly greater concentrations than Mg (Table 3).

At Rio Icacos, normalized Mg concentrations (C_w) remain consistently low throughout the saprolite relative to bedrock C_0 (Table 3). This situation is attributed to the near-complete weathering of hornblende and the loss of Mg in biotite at the bedrock/saprolite interface (Table 2). In contrast, K concentrations in the saprolite are comparable to that of the regolith. K is lost only at relatively shallow depths in the soil horizons (Table 2). Although K is also mobilized during biotite, it must be retained in the regolith, possibly by sorption to secondary clay and Fe-oxide phases (White et al., 1998). Thus, while the solid-state Mg and K distributions in the Panola regoliths are applicable for calculating a biotite weathering rate based on Eq. (16), corresponding solid-state Mg and K distributions in the Rio Icacos regolith are not.

3.3. Solute weathering gradients

Representative pore water compositions in the Panola and Rio Icacos saprolites are presented in Table 4. Solute Mg and K exhibit significant variability in the shallow soils in both the Panola and Rio Icacos regoliths due to seasonal patterns in precipitation, evapotranspiration and selective addition and removal by biologic cycling (White et al., 2002). Immediately below the soil zones, solute concentrations are generally lower and more consistent. Mg and K in Rio Icacos pore waters increase downward from this depth, signifying progressive increases due to chemical weathering of biotite (Fig. 8).

The distribution of pore water Mg and K with depth in the Rio Icacos regolith (Fig. 8) defines the solute weathering gradient (Fig. 1). Due to significant variability in the soil horizon, linear regression fits are confined to pore water Mg and K increases from the top (c_0) to the base (c_w) of the underlying saprolite (c_w). The slope for the Mg regression in Fig. 8 is $b_p = 1.13 \times 10^5$ m l mol^{-1} ($r = 0.69$) and the slope for K is $b_p = 1.96 \times 10^5$ m l mol^{-1} ($r = 0.91$). The weathering gradient for Mg is shallower than for K indicating that Mg is weathering from the regolith faster than is K. The relative ratio of release rates is equal to the inverse of their slopes or 1.73. This ratio approximates the ratio of the stoichiometric coefficients β of Mg to K for unweathered biotite in the bedrock (1.47) but is significantly higher than the ratios of Mg to K in the weathered biotite in the Rio Icacos saprolite (0.85) (Table 2).

Table 4
Representative chemical compositions of precipitation and pore waters in the Panola and Rio Icacos regoliths

	Precipitation				Regolith pore water							
	Panola		Rio Icacos		Panola				Rio Icacos			
	Open fall	Thru fall	Open fall	Thru fall	0.9 m	1.8 m	3.0 m	4.6 m	1.2 m	3.6 m	6.7 m	8.5 m
pH	4.83	4.05	5.6	5.2	5.5	5.4	5.4	5.6	4.0	4.3	5.6	5.1
Na	11.4	10.6	59.2	119	40.0	202	206	163	90.2	132	187	156
K	1.8	10.6	1.4	12.3	36.2	43.7	17.7	12.9	5.2	9.3	24.5	39.5
Ca	3.3	32	3.8	6.8	25.5	24.1	12.5	14.5	12.7	7.3	12.8	27.2
Mg	1.7	19.2	19.2	13.2	81.7	66.5	56.4	35.2	18.9	23.6	33.5	59.3
Al	na	na	na	0.0	4.0	0.9	2.3	4.7	9.0	2.0	0.0	15.6
Si	na	na	0.0	0.0	92.9	201	189	372	60.7	86.0	221	216
Cl	14.1	20.6	64.9	163	34.1	251	319	202	128	178	142	171
NO_3	31.6	19.3	0.0	0.0	1.1	23.8	2.8	2.1	0.0	3.4	14.9	18.9
SO_4	36.8	42.7	6.9	15.4	43.9	10.3	1.6	6.1	12.4	7.2	7.5	7.6
Alk	0.0	0.0	0.0	0.0	63.4	30.8	25.4	55.6	0.0	0.0	64.0	67.6

Units are in μM except as noted (after White et al., 1998, 2002).

In the Panola regolith, solute Mg and K concentrations remain low or actually decrease with depth in the saprolite, denoting a lack of any apparent weathering input from biotite (White et al., 2002). The difference in the behavior of Mg and K in the Panola and Rio Icacos pore waters is attributed to different patterns of nutrient uptake by the forest covers. The deeper Luquillo regolith is closed to biological uptake of inorganic nutrients such as Mg and K, produced by weathering, due to the shallow rooting depth of the rainforest vegetation. This closed system cycling is consistent with other tropical environments in which soil mineral nutrient balances for vegetative covers are shown to be spatially consistent over differing bedrock types (Hamdan and Burnham, 1996).

In contrast to Luquillo, the more temperate Panola regolith is an example of an open system in which base cations, principally K and Mg released from biotite weathering, are removed due to biological uptake. In the Panola regolith, the predominance of tree roots is in the soil horizon but a lower density of roots is observed to penetrate to the bedrock. The uptake by deeper rooting systems associated with more temperate forest cover, coupled with the shallower thickness of saprolite, is sufficient to quantitatively remove mineral nutrients. This process is accelerated for Panola since the forest is aggrading due to past logging and other land use activities (Huntington et al., 2000). Although biotite is currently weathering in the Panola regolith, biological processes overwhelm Mg and K contributions to pore waters. This prevents the calculation of Panola biotite weathering rates based on solute distributions plotted in Fig. 8.

3.4. Biotite surface areas

As discussed by White and Peterson (1990) and Brantley et al. (1999), accurate characterization of surface areas of naturally weathered minerals is difficult and is the parameter which may introduce the single largest error in the calculation of natural weathering rates. Biotite BET surface areas (s in Eq. (15)), range between 1.5 and 7 $m^2\ g^{-1}$ for Panola (White et al., 2002) and 8.1 and 8.3 $m^2\ g^{-1}$ for Rio Icacos (Murphy et al., 1998). These surface areas exhibit no consistent trend with depth but are significantly greater than a range of 0.24 and 5.6 $m^2\ g^{-1}$ reported for fresh biotites (Acker and Bricker, 1992; Kalinowski and Schweda, 1996; Malmstrom and Bainwat, 1997; Taylor et al., 2000). Part of this difference is attributed to the epitaxial replacement of biotite by high surface area kaolinite in the regoliths on a scale, which precludes physical separation (Fig. 3). Specific surface areas (s) of 5.0 and 8.2 $m^2\ g^{-1}$ are used, respectively, in the Panola and Rio Icacos rate calculations (Eqs. (16) and (17)).

The volumetric surface area S, which describes the surface area of biotite per unit volume of regolith, is

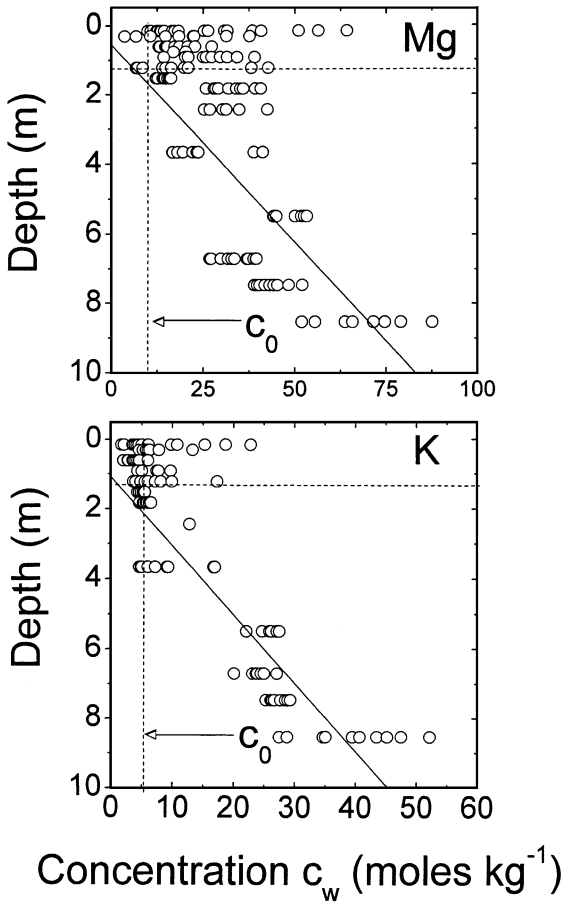

Fig. 8. Normalized pore water Mg and K concentrations (c_w) plotted as a function of depth in the Rio Icacos regolith. Horizontal dashed lines are approximate contacts between the soil and underlying saprolite horizons. C_0 is the measured protolith concentrations (vertical dashed lines). The diagonal lines are the linear regression fits describing the pore water weathering gradients b_p (Eq. (17)).

related to the specific biotite surface area s by the regolith density and the weight fraction of biotite in the regolith ϕ (Eq. (15)). Regolith densities ρ_w are reported in Table 3. Values for ϕ are calculated from the stoichiometries and molar weights of biotite (Table 2) and the Mg concentrations in the regolith (Table 3). In the Rio Icacos regolith, Mg is only contained in the weathered biotite. In the Panola regolith, the residual biotite fraction is calculated by first subtracting out the Mg component in muscovite assuming that it does not weather and is contained in the regolith in the same abundance as in bedrock (Table 2). As shown in Table 3, the biotite weight fractions ϕ for the Panola and Rio Icacos regoliths are comparable.

3.5. Determination of weathering velocities

The weathering velocity in the solid regolith ω (m s^{-1}) corresponds to the rate at which the weathered regolith is propagating into the unweathered protolith. This rate is calculated from age dating of the regolith surface assuming static equilibrium between the rates of propagation of the weathering front and physical denudation at the surface. Such conditions are commonly approached during long-term saprolitic weathering (Cleaves et al., 1974; Pavich, 1986). Under such conditions, the regolith thickness remains constant. The weathering velocity ω is derived by dividing this thickness by the age of the regolith surface, i.e. $\omega = z/t$. Based on cosmogenic ^{36}Cl distributions, Bierman et al. (1995) established ages of between 2 and 5×10^5 years for surficial outcrops of the Panola granite in the watershed. This results in an average regolith denudation rate of 10 m/10^6 years and a solid-state weathering velocity ω of 3.2×10^{-13} m s^{-1}. Based on ^{10}Be measurements of soil and rock surfaces in the Rio Icacos watershed, Brown et al. (1995) estimated a steady-state denudation rate of 25 m/10^6 years with translates into a solid-state weathering velocity ω of 7.9×10^{-13} m s^{-1}.

The weathering velocity for the solute corresponds to the rate of pore water infiltration through the regolith. Under constant conditions of pressure head, Darcy's Law requires that the flux density q_h (Eq. (12)) is equal in magnitude and opposite in sign to the hydraulic conductivity K_s. As discussed by Stonestrom et al. (1998) and White et al. (2002), the soil/saprolite interface at a depth of 1.5 m in the Panola regolith consists of a duripan that restricts the downward percolation of water. Flow in this region occurs at or near saturated conditions throughout most of the year. Saturated hydraulic conductivites, measured in cores taken from this zone, produced an average vertical infiltration rate of $q_h = 1.4 \times 10^{-8}$ m s^{-1}. A simple water balance between average annual precipitation and Panola watershed discharge results in a comparable infiltration rate of $q_h = 1.2 \times 10^{-8}$ m s^{-1}. Based on experimental unsaturated conductivities in the Rio Icacos saprolite, an infiltration rate of $q_h = 3.4 \times 10^{-8}$ m s^{-1} was derived (White et al., 1998; Stonestrom et

al., 1998). This is in relatively close agreement with an infiltration rate of $q_h = 2.1 \times 10^{-8}$ m s^{-1} based on averaging base discharge in the Rio Icacos watershed.

3.6. Calculation of weathering rates

The parameters determined in the preceding sections permit the calculation of the weather rates of biotite based on solid and solute weathering gradients and velocities, The specific data used for the rate equations (Eqs. (16) and (17)) are tabulated in Table 5. The weathering rates for biotite are $R = 3.3$ and 6.8×10^{-17} mol m^{-2} s^{-1} based on respective solid Mg and K weathering gradients in the Panola regolith (Fig. 7). The faster K rate is attributable to an additional K-feldspar contribution to weathering. The biotite weathering rates in the Rio Icacos are $R = 3.6$ and 1.8×10^{-16} mol m^{-2} s^{-1} based on solute Mg and K weathering gradients (Fig. 8). The slower biotite rate for K may be due preferential retention by sorption on secondary clay and Fe oxides. The observation that the overall biotite weathering rates are more rapid in the Rio Icacos watershed compared to the Panola watershed is consistent with higher temperatures and greater precipitation, which promote a more aggressive weathering environment.

4. Discussion

The preceding sections describe parallel methodologies for calculating natural mineral weathering rates based on measured changes in solid and pore water elemental concentrations with depth. The following sections discuss the similarities and differences in the calculations and implications for natural weathering studies.

4.1. Role of physical parameters

A comparison of Eqs. (16) and (17) shows that both the solute and solid-state weathering rate expressions are inversely proportional to the product of the regolith density ρ the mineral fraction ϕ and the

Table 5
Parameters used to calculate biotite weathering rates based on Eqs. (16) and (17)

Parameter	Symbol	Units	Panola	Rio Icacos	Source
Weathering gradients					
Solid-state Mg	b_s	m mol^{-1} kg^{-1}	2.5×10^{1}	nd	Normalized C_w versus depth (Fig. 7)
Solid-state K	b_s	m mol^{-1} kg^{-1}	1.1×10^{1}	nd	Normalized C_w versus depth (Fig. 7)
Solute Mg	b_p	m mol^{-1} l^{-1}	nd	1.1×10^{5}	Pore water c_w versus depth (Fig. 8)
Solute K	b_p	m mol^{-1} l^{-1}	nd	2.0×10^{5}	Pore water c_w versus depth (Fig. 8)
Weathering velocities					
Solid-state	q_h	m^3 m^{-2} s^{-1}	1.3×10^{-8}	2.6×10^{-8}	Denudation based on cosmogenic isotope age dates
Solute	ω	m s^{-1}	3.2×10^{-13}	7.9×10^{-13}	Measured infiltration rates
Regolith properties					
Density	ρ_w	g cm^{-3}	1.91	1.27	Average of measured densities (Table 3)
Stiochiometric coefficent/Mg	β	mol mol^{-1}	0.89	0.55	Weathering reactions (Eqs. (18) and (19))
Stiochiometric coefficent/K	β	mol mol^{-1}	0.98	0.65	Weathering reactions (Eqs. (18) and (19))
Biotite specific surface area	s	m^2 g^{-1}	5.00	8.20	Average of BET surface areas
Biotite mass fraction	ϕ	kg kg^{-1}	0.087	0.110	Solid state Mg and biotite stiochiometry (Tables 2 and 3)
Biotite weathering rates					
Solid-state Mg	R_s	mol m^{-2} s^{-1}	3.3×10^{-17}	nd	Rate expression (Eq. (16))
Solid-state K	R_s	mol m^{-2} s^{-1}	6.7×10^{-17}	nd	Rate expression (Eq. (16))
Solute Mg	R_p	mol m^{-2} s^{-1}	nd	3.6×10^{-16}	Rate expression (Eq. (17))
Solute K	R_p	mol m^{-2} s^{-1}	nd	1.8×10^{-17}	Rate expression (Eq. (17))

mineral surface area s. Rate calculations based on solute gradients (Eq. (17)) require one additional term in the calculation, the specific regolith density ρ. For solute gradients, these physical parameters are expected to vary spatially with depth in the regolith but not temporally due to the relatively short fluid residence times involved. Calculating the weathering rates based on relatively large depth intervals is advantageous due to significant changes in elemental concentrations. Solute Mg and K concentrations increased by an order of magnitude from the shallowest to deepest portions of the Panola and Rio Icacos regoliths. Regression fits to such composition changes provide a robust method for determining the weathering gradients employed in Eqs. (16) and (17).

This advantage is offset, somewhat, by changes in physical properties over the same depth interval, produced in part, by long-term chemical weathering (Fig. 6). Average values for these parameters are used for calculating the biotite weathering rates in the Rio Icacos and Panola regoliths (Table 5). One approach to overcoming spatial variations in mineral content and surface area is to link them with the progress of mineral reaction (Helgeson et al., 1984). Recently, White et al. (2001) used this approach to determine rates of feldspar weathering in the Panola regolith. The linearity in the weathering gradients with depth implies that the rate of element losses in the solid and solute cannot be directly proportional to changes in mineral abundances. Decreases in mineral fractions may be counteracted by the specific surface area, which is shown to increase with weathering under experimental and natural conditions due to increases in surface roughness and intergranular porosity (White et al., 1996; Brantley et al., 1999).

4.2. Comparison of weathering gradients and velocities

Under ideal long-term steady-state conditions, the chemical weathering rate of a mineral should be identical whether it is calculated based on solute or solid-state distributions, i.e. $R_s = R_p$. Equating Eqs. (16) and (17) produces the expression

$$\frac{b_s}{b_p} = \rho_w \frac{\omega}{q_h} \tag{21}$$

in which the ratio of the solid to solute weathering gradients is inversely proportional to the ratio of the corresponding weathering velocities.

While the magnitudes of the ratios of the respective solute and solid gradients and velocities must be similar (Eq. (21)), the individual values are very different. As indicated in Table 5, the solute gradients (b_p) for the Rio Icacos regolith are approximately four orders of magnitude greater than for the corresponding solid gradients for the Panola (b_s). This translates into a much smaller increase in the solute element mass with depth in the Rio Icacos pore water relative to solute state increases in the Panola regolith. In contrast, the solute weathering velocity based on the fluid flux density (Table 5 is approximately four orders of magnitude faster than the solid-state weathering velocity). This difference is attributed to very different time scales over which weathering occurs. Pore water residence times in the Rio Icacos and Panola regoliths are estimated to be 8 to 12 years (White et al., 2002). In contrast, the times associated with solid-state weathering in the Panola and Rio Icacos regoliths are estimated to be between 2 and 5×10^5 years (Brown et al., 1995; Bierman et al., 1995). During such times, hundreds of thousands of pore water volumes have infiltrated through the two regoliths.

In spite of the differences in the scales of weathering gradients and velocities, Eq. (21) predicts that under steady-state conditions, the solute and solid-state weathering rates will be equal for a given weathering environment. Although the results of the present study compares biotite weathering rates in different environments, the magnitude of the difference in weathering rates is still relatively small, The biotite weathering rate at Rio Icacos based on solute weathering gradients is about five times faster than for Panola based on solid-state gradients. This difference is in agreement with a warmer and wetter tropical climate in Puerto Rico.

4.3. Comparsion of biotite weathering rates

The weathering rates of biotite in the Panola and Rio Icacos regoliths are compared to both natural and experimental dissolution rates reported elsewhere in the literature (Table 6). Reported pH ranges, methods of surface area determination and elemental basis for

Table 6
Weathering rates of biotite measured in field and laboratory studies

Log rate R, mol m^2 s^{-1}	pH	Location or experiment	Surface area	Basis of rate determination	Reference
Field					
− 16.5	5.0–5.5	Panola, GA, USA	BET	Solid Mg gradient	This paper
− 16.2	5.0–5.5	Panola, GA, USA	BET	Solid K gradient	This paper
− 15.4	4.5–5.5	Luquillo, Mtn. PR	BET	Solute Mg gradient	This paper
− 15.7	4.5–5.5	Luquillo, Mtn. PR	BET	Solute Mg gradient	This paper
− 16.4	5.0–5.5	Panola, GA, USA	BET	Mg regolith loss	White et al. (2002)
− 15.0	4.5–5.5	Luquillo, Mtn. PR	BET	Mg solute flux	Murphy et al. (1998)
− 14.1	7.0	Loch Vale, CO, USA	BET	Cation flux	Clow and Drever (1996)
− 14.0	4.5	Bear Brook, MA, USA	Geometric	Si solute flux	Swodoba-Colberg and Drever (1993)
− 13.0	6.0	Coweeta, NC, USA	Geometric	Mg release	Velbel (1985)
Laboratory					
− 13.0	7.0	Experimental	BET	Cation release	Clow and Drever, 1996
− 11.9	4.5	Experimental	BET	Cation release	Kalinowski and Schweda (1996)
− 11.6	3.0	Experimental	BET	K and Mg release	Taylor et al. (2000)
− 11.5	4.0–4.5	Experimental	BET	K and Mg release	Sverdrup and Warfvinge (1995)
− 11.2	5.0	Experimental	BET	K and Mg release	Malmstrom and Bainwat (1997)
− 11.4	4.5	Experimental	Geometric	K release	Swodoba-Colberg and Drever (1993)
− 10.7	5.0	Experimental	BET	Mg release	Acker and Bricker (1992)

the biotite rate constants are also tabulated. As indicated, the biotite weathering rates calculated from solid and solute weathering gradients in the present study are in agreement with rates calculated by Murphy et al. (1998) for the Rio Icacos regolith and by White et al., 2002 for the Panola regolith. This is expected since the rates are based on similar sets of parameters measured in these regoliths.

Weathering rates for Panola and Rio Icacos biotites are three to six orders of magnitude slower than the reported experimental rates. This large discrepancy is even greater than that reported for other silicates such as feldspars (Schnoor, 1990; Brantley, 1992; White et al., 2002) and is probably related to the fact that short-term experiments based on fresh biotite are susceptible to relatively fast oxidation and interlayer diffusion. Such experimental studies predict that biotite would be weathered from regoliths on the time scale of hundreds to thousands of years. During natural weathering, biotite is one of the most stable silicate phases and persists in Panola and Rio Icacos regoliths for several hundred thousand years.

The biotite weathering rates in the Panola and Rio Icacos regoliths are also significantly slower than the natural field rates reported by Velbel (1985) and Swodoba-Colberg and Drever (1993). Both these studies estimated the specific biotite surface area from particle sizes. Such geometric estimates have been shown to be one to two orders of magnitude less than BET surface areas (Brantley, 1992; White et al., 2002).

5. Summary

This work presents a systematic approach to calculating chemical weathering rates of silicate minerals in soil and regoliths. Although calculations, based on solid and pore water distributions exist in the literature, this is the first effort to integrate the approaches into a form that permits direct comparsions of the parameters employed and reveals potential errors and limitations involved. The approach utilizes the concept of weathering gradient, which describes the solid and solute distributions of an element with depth in the regolith. The slopes of these gradients, which under steady-state weathering conditions, are described statistically by linear regression analyses, are a dynamic function of the

weathering rate, which increases the change in element concentrations with depth, and the weathering velocity which decreases the concentration change with depth. The solid weathering velocity is the propagation rate of the weathering front into the protolith and the solute weathering velocity is the fluid flux density. Solute concentrations correlate directly with pore water values while solid concentrations must be normalized with respect to an inert component such as Ti in order to correct for regolith density and volume changes resulting from weathering.

The solid and solute weathering gradients are proportional to the ratios of the respective weathering velocities and gradients. Under steady-state conditions, the long-term solid weathering rate must equal to the short-term solute rate, thereby requiring similar values from the respective velocity/gradient ratios. In the case of the solute rate, this ratio corresponds to dividing a relatively rapid weathering velocity by a steep weathering gradient. In the case of the solid-state rate, the ratio corresponds to dividing a slow weathering velocity by a shallow weathering gradient. The rates are also both proportional to physical parameters, which describe chemical and physical distributions in the regolith including reaction stoichiometry, mineral abundance and specific mineral surface area. The solute rate is dependent on one additional feature, the regolith density. These parameters change with regolith depth and weathering intensity. However, the common observation that weathering gradients are linear in soil profiles suggests that changes in these physical parameters compensate each other. One possible inverse correlation is between mineral abundance which decreases and specific surface area which increases during weathering.

The above approach is applied to biotite weathering rates in the saprolitic regoliths developed on granitoid rocks. Linear solid-state Mg and K weathering gradients due to biotite weathering are determined in the Panola watershed of Georgia, USA. Solute gradients in the pore waters are not present due to the overwhelming effect of macronutrient uptake by the forest cover. In contrast, linear solute Mg and K gradients exist in the Rio Icacos watershed in Puerto Rico due to biotite weathering. Biological uptake of these elements does not occur due to shallow rooting depth of the tropical vegetation and the thick sequence of saprolite. Solid-state linear gradients do not exist in the Rio Icacos due to the complex stoichiometry of biotite weathering. Resulting weathering rates are approximately five times faster at Rio Icacos than at Panola as expected based on a significantly wetter and warmer climate. These rates are up to six orders of magnitude slower than experimental rates of biotite weathering, implying that calculations based on natural elemental distributions in soils and regoliths or in associated pore waters may be the only realistic approach to calculating natural weathering rates.

Acknowledgements

The author expresses his appreciation to a number of individuals who collaborated on studies at the Panola and Rio Icacos watersheds. These include Alex Blum, Tom Bullen, Tom Huntington, Mathew Larson, Norman Peters, Marjorie Schulz and Davison Vivit of the US Geological Survey and Susan Brantley and Shelia Murphy of The Pennsylvania State University. The Watershed Energy Biochemical Budgets Program (WEBB) of the Water Resources Division of the US Geological Survey provided the funding for this work. **[EO]**

References

Acker, J.G., Bricker, O.P., 1992. The influence of pH on biotite dissolution and alteration kinetics at low temperature. Geochimica et Cosmochimica Acta 56, 3073–3092.

Banfield, J.F., Eggleton, R.A., 1988. Transmission electron microscope study of biotite weathering. Clays and Clay Minerals 36, 47–60.

Berner, R.A., Berner, E.K., 1997. Silicate weathering and climate. In: Ruddiman, W.F. (Ed.), Tectonic Uplift and Climate Change. Plenum, New York, pp. 353–364.

Bierman, P., Gillespie, A., Caffee, M., Elmore, D., 1995. Estimating erosion rates and exposure ages with ^{36}Cl produced by neutron activation. Geochimica et Cosmochimica Acta 59, 3779–3798.

Brantley, S.L., 1992. Kinetics of dissolution and precipitation—experimental and field results. In: Kharaka, Y., Maest, A. (Eds.), Water–Rock Interaction 7. A.A. Balkema, Park City, Rotterdam, pp. 465–469.

Brantley, S.L., White, A.F., Hodson, M.E., 1999. Surface area of primary silicate minerals. In: Jamtveit, B., Meakin, P. (Eds.), Growth, Dissolution and Pattern Formation in Geosystems. Kluwer Academic Publishing, pp. 291–326.

Brown, E.T., Stallard, R.F., Larsen, M.C., Raisbeck, G.M., Yiou, F., 1995. Denudation rates determined from the accumulation of in situ produced ^{10}Be in the Luquillo Experimental Forest, Puerto Rico. Earth and Planetary Science Letters 129, 193–202.

Cleaves, E.T., Fisher, D.W., Bricker, O.P., 1974. Chemical weathering of serpentinite in the eastern piedmont of Maryland. Geological Society of America Bulletin 5, 437–444.

Clow, D.W., Drever, J.I., 1996. Weathering rates as a function of flow through an alpine soil. Chemical Geology 132, 131–141.

Dong, H., Peacor, D.R., Murphy, S.F., 1998. TEM study of progressive alteration of igneous biotite to kaolinite throughout a weathered soil profile. Geochimica et Cosmochimica Acta 62, 1881–1887.

Drever, J.I., Hurcomb, D.R., 1986. Neutralization of atmospheric acidity by chemical weathering in an alpine drainage basin in the North Cascade Mountains. Geology 14, 221–224.

Garrels, R.M., Mackenzie, F.T., 1967. Origin of the chemical composition of some springs and lakes. In: Stumm, W. (Ed.), Equilibrium Concepts in Natural Water Systems. Amer. Chem. Soc Adv. Chemistry Ser., vol. 67, pp. 222–242.

Hamdan, J., Burnham, C.P., 1996. The contribution of nutrients from parent material in three deeply weathered soils of Peninsular Malaysia. Geoderma 74, 219–233.

Helgeson, H.C., Murphy, W.M., et al., 1984. Thermodynamic and kinetic constraints on reaction rates amoung minerals and aqueous solutions, II. Rate constants, effective surface area, and the hydrolysis of feldspar. Geochimica et Cosmochimica Acta 48, 2405–2432.

Hillel, D., 1982. Introduction to Soil Physics. Academic Press, Orlando, 345 pp.

Huntington, T.G., Hooper, R.P., Johnson, C.E., Aulenbach, B.T., Cappellato, R., Blum, A.E., 2000. Calcium depletion in forest ecosystems of the southeastern United States. Soil Science Society of America Journal 64, 1845–1858.

Kalinowski, B.E., Schweda, P., 1996. Kinetics of muscovite, phlogopite and biotite dissolution and alteration at pH 1–4 and room temperature. Geochimica et Cosmochmica Acta 60, 367–385.

Kenoyer, G.J., Bowser, C.J., 1992. Groundwater chemical evolution in a sandy silicate aquifer in Northern Wisconsin 2. Reaction modeling. Water Resources Research 28, 591–600.

Malmstrom, M., Bainwat, S., 1997. Biotite dissolution at 25 °C: the pH dependence of dissolution rate and stoichiometry. Geochimica et Cosmochimica Acta 61, 2779–2799.

Murphy, S.F., Brantley, S.L., Blum, A.E., White, A.F., Dong, H., 1998. Chemical weathering in a tropical watershed, Luquillo Mountains, Puerto Rico: II. Rate and mechanism of bioitite weathering. Geochimica et Cosmochimica Acta 62, 227–243.

Paces, T., 1986. Rates of weathering and erosion derived from mass balance in small drainage basins. In: Dethier, S.M., Colman, D.P. (Eds.), Rates of Chemical Weathering of Rocks and Minerals. Academic Press, Orlando, pp. 531–550.

Pavich, M.J., 1986. Processes and rates of saprolite production and erosin on a foliated granitic rock of the Virginia Piedmont. In: Colman, S.M., Dethier, D.P. (Eds.), Rates of Chemical Weathering of Rocks and Minerals. Academic Press, Orlando, pp. 551–590.

Plummer, L., Prestemon, E.C., Parkhurst, D.L., 1991. An interactive code (NETPATH) for modeling net geochemical reactions along a flow path. U.S. Geological Survey Water-Resources Investigation Reports 91–4078, 227 pp.

Schnoor, J.L., 1990. Kinetics of chemical weathering: a comparison of laboratory and field rates. In: Stumm, W. (Ed.), Aquatic Chemical Kinetics. Wiley, Interscience, New York, pp. 475–504.

Stonestrom, D.A., White, A.F., Akstin, K.C., 1998. Determining rates of chemical weathering in soils—solute transport versus profile evolution. Journal of Hydrology 209, 331–345.

Sverdrup, K., Warfvinge, P., 1995. Estimating field weathering rates using laboratory kinetics. In: White, A.F., Brantley, S.L. (Eds.), Chemical Weathering Rates of Silicate Minerals, vol. 31. Mineralogical Society of America Reviews in Mineralogy, vol. 31, pp. 485–539.

Swodoba-Colberg, N.G., Drever, J.D., 1993. Mineral dissolution rates in plot-scale field and laboratory experiments. Chemical Geology 105, 51–69.

Taylor, A.S., Blum, J.D., Lasaga, A.C., MacInnis, I.N., 2000. Kinetics of dissolution and Sr release during biotite and phlogopite weathering. Geochimica et Cosmochimica Acta 64, 1191–1208.

Velbel, M.A., 1985. Geochemical mass balances and weathering rates in forested watersheds of the southern Blue Ridge. American Journal of Science 285, 904–930.

Velbel, M.A., 1986. The mathematical basis for determining rates of geochemical and geomorphic processes in small forested watersheds by mass balance: examples and implications. In: Colman, S.M., Dethier, D.P. (Eds.), Rates of Chemical Weathering of Rocks and Minerals. Academic Press, Orlando, pp. 439–449.

Velbel, M.A., 1990. Mechanisms of saprolitization, isovolumetric weathering and pseudomorphous replacement during rock weathering—a review. Chemical Geology 84, 17–19.

White, A.F., 1995. Chemical weathering rates in soils. In: White, A.F., Brantley, S.L. (Eds.), Chemical Weathering Rates of Silicate Minerals, vol. 31. Mineralogical Soc. Am., pp. 407–458.

White, A.F., Claassen, H.C., 1978. Dissolution kinetics of silicate rocks, application to solute modeling. In: Jenne, E. (Ed.), Speciation, Sorption, Solubility and Kinetics in Aqueous Systems. Amer. Chem. Soc. Symp. Series, vol. 93, pp. 771–793.

White, A.F., Peterson, M.L., 1990. Role of reactive surface area characterization in geochemical models. In: Mechlior, D.C., Bassett, R.L. (Eds.), Chemical modeling of aqueous systems II. ACS Symp. Series, vol. 416, pp. 461–475.

White, A.F., Blum, A.E., Schulz, M.S., Bullen, T.D., Harden, J.W., Peterson, M.L., 1996. Chemical weathering of a soil chronosequence on granitic alluvium: 1. Reaction rates based on changes in soil mineralogy. Geochimica et Cosmochimica Acta 60, 2533–2550.

White, A.F., Blum, A.E., Schulz, M.S., Vivit, D.V., Larsen, M., Murphy, S.F., 1998. Chemical weathering in a tropical watershed, Luquillo Mountains, Puerto Rico: I. Long-term versus short-term chemical fluxes. Geochimica Cosmochiica Acta 62, 209–226.

White, A.F., Bullen, T.D., Blum, A.E., Schulz, M.S., Huntington, T.G., Peters, N.E., 2001. Differential rates of feldspar weathering in granitic regoliths. Geochimica et Cosmochimica Acta 65, 847–869.

White, A.F., Blum, A.E., Schulz, M.S., Huntington, T.G., Peters, N.E., Stonestrom, D.A., 2002. Chemical weathering of the Panola Granite: solute and regolith elemental fluxes and the dissolution rate of biotite. In: Hellmann, R., Wood, S.A. (Eds.), Water-rock Interaction, Ore Deposits, and Environmental Geochemisty: A tribute to David A. Crerar Special Publ. 7. The Geochemical Society St. Louis, pp. 37–60.